

Vibronic mode couplings in adsorbed molecules analyzed by doubly resonant sum-frequency generation

J. C. Vallet

Scuola Normale Superiore, Piazza dei Cavalieri 7, I-56126 Pisa, Italy

A. J. Boeglin, J. P. Lavoine, and A. A. Villaeys

Institut de Physique et Chimie des Matériaux de Strasbourg, Groupe d'Optique Nonlinéaire et d'Optoélectronique, 23 rue du Loess, 67037 Strasbourg Cedex, France

(Received 27 November 1995)

We present multimode model calculations of doubly resonant infrared-visible sum-frequency generation from adsorbed molecules with general harmonic potential surfaces that are valid for finite temperatures. Numerical simulations of spectra recorded versus the frequency of the infrared or the visible sources have been performed on a simple two-mode model with equilibrium position displacements, frequency shifts, and Duschinsky rotation upon electronic excitation. It is argued that quadratic vibronic couplings need to be included if the excited state potential well is to be reliably probed by these techniques. [S1050-2947(96)03006-5]

PACS number(s): 42.65.Ky, 63.35.Ja

I. INTRODUCTION

Molecules adsorbed at surfaces are being studied intensively to understand physical as well as chemical processes. The observation of vibrational spectra of adsorbed species is the common feature of a variety of experimental methods used to characterize many surface properties [1]. Identifying adsorbed species, probing their orientations and interactions with each other or with the substrate are all essential steps to furthering our understanding of the physics and the chemistry of surfaces and interfaces. While doubly resonant infrared-visible sum-frequency generation (DR IRVSFG) also falls into the broad category of vibrational spectroscopy, we will study it here in the context of a well defined application, namely the probing of the excited state potential surface of an adsorbed molecule. Here, the emphasis is less on surface physics and chemistry than on the study of the properties of well oriented molecules in contact with an environment as a test case for optical properties of molecules in condensed phases.

The use of DR IRVSFG, as well as that of difference-frequency generation (DR IVDFG) to investigate the coupling between electronic states and vibrational modes in molecules on surfaces, has been recently proposed by Huang and Shen [2]. These authors have shown that these techniques are highly sensitive to the vibrational structure of the adsorbed species while detecting the signal in the visible frequency range. Compared to other techniques, one great advantage of this type of experiments lies in its high surface specificity. In their theoretical description, Huang and Shen have only considered the case of the linear vibronic coupling.

In the field of Raman spectroscopy, the developments of the formal theory are often based on the expression derived by Kramers, Heisenberg, and Dirac involving dipole-moment matrix elements between vibronic states and energy denominators. Within the usual approximations, the overlaps between the vibrational states, i.e., the Frank-Condon fac-

tors, carry all the information about the relative shapes of the ground and excited state potential wells. Heller [3] has shown that an equivalent time-dependent theory focusing on the motion of the wave packet created in the intermediate excited state of the molecule provides a more intuitive description, especially if one wants to grasp the essential differences between an off-resonance experiment and resonance Raman scattering. In a sense, the closer to resonance one performs the experiment, the larger the area of the excited state potential surface that is being probed, so that general harmonic surfaces need to be considered [4]. In the field of infrared-visible sum-frequency generation (IVSFG) [5], a technique being used to study the ground state vibrational properties of molecular adsorbates, the situation may be quite analogous, although only experiments where the visible excitation is off-resonance with respect to the electronic transition are routinely being carried out.

The papers by Mukamel *et al.* [6] and by Deng *et al.* [7] were among the pioneering works concerned with the influence of mode mixing within the Condon approximation on the nonlinear optical susceptibilities and coherent Raman line shapes in large molecules. A closed form expression of two-dimensional Franck-Condon overlap integrals under mode mixing has been derived recently [8]. Also, the structural and dynamical consequences of the rotational Duschinsky effect [9] on the absorption spectra of 2-pyridone have been analyzed [10]. A few years ago, Hizhnyakov and Tehver [11] had proposed a description of linear and quadratic electron-phonon coupling in first-order resonance Raman scattering. However, their approach, based on the density matrix for a multidimensional harmonic oscillator, and reminiscent of a previous derivation of Kubo and Toyozawa of an optical absorption time-correlation function for linear and quadratic couplings [12], is valid solely at zero temperature as it includes transition amplitudes from the lowest vibrational state only.

Page *et al.* [13–19] have developed a general formalism for treating vibrational mode mixing, also referred to as the

Duschinsky rotation [9], frequency shifts, and nuclear equilibrium position shifts under electronic excitation. They have demonstrated that the interpretation of resonance Raman scattering (RRS) experiments requires the introduction of quadratic coupling terms responsible for frequency shifts and vibrational mode mixing [14–16]. We will take advantage of the diagrammatic technique they developed for RRS [14–19], to derive analytical results which allow the evaluation of DR IVSFG spectra for molecules with general harmonic potential surfaces. Thus, we extend the model of Huang and Shen to a linear plus quadratic vibrational Hamiltonian [20]. Again, this approach is different from the standard sum-over-state method with its overlap integrals, but it leads to analytical expressions which are not only exact, but valid for an arbitrary number of modes and for finite temperatures.

It is the goal of the present work to give a complete account of second order optical responses of adsorbed molecular systems with general quadratic vibronic couplings that is valid for finite temperatures. For simplicity, we have considered the case of a molecule characterized by two electronic states and two vibrational modes. We will show that one difficulty which must be overcome when interpreting experimental spectra lies in the discrimination between linear and quadratic effects. We will do so by simulating the problem of parameter recovery from a set of model calculations [21]. Our aim is to prove the ability of DR IVSFG experiments to discriminate between linear and quadratic electron-phonon couplings provided that one records a full set of spectra corresponding to all the active vibrational modes involved. With the help of this information, one can then hope to get access to the excited state potential wells of adsorbed species, thus laying the groundwork for the study of excited state dynamics in such systems.

The paper is organized as follows. In Sec. II, the formal description of the molecular system and the SFG process is presented. It involves the introduction of matrices to handle properly the shifts in equilibrium positions, the changes in vibrational frequency and the amount of mode mixing upon electronic excitation, as well as the derivation of the expression of the SFG time correlator. In Sec. III, we briefly outline the diagrammatic expansion of the SFG time correlator and state the analytical expressions used in our study of DR IRVSFG spectra. In Sec. IV, we first illustrate the effects of the molecular parameters on these spectra with numerical calculations on a simple model system, then we examine the possibility of recovering linear and quadratic coupling constants from such data, and last we look at the influence of temperature. Finally, we state our conclusions in the final section.

II. THEORY

The theoretical framework required to evaluate the SFG signal emitted by molecules is introduced in the present section. To this end, the dynamical evolution of the density matrix $\rho(t)$ corresponding to the molecular system interacting with the light fields is governed by the Liouville equation [6,22–28]

$$\frac{\partial \rho(t)}{\partial t} = -\frac{i}{\hbar} L'_0 \rho(t) - \frac{i}{\hbar} L_v(t) \rho(t), \quad (1)$$

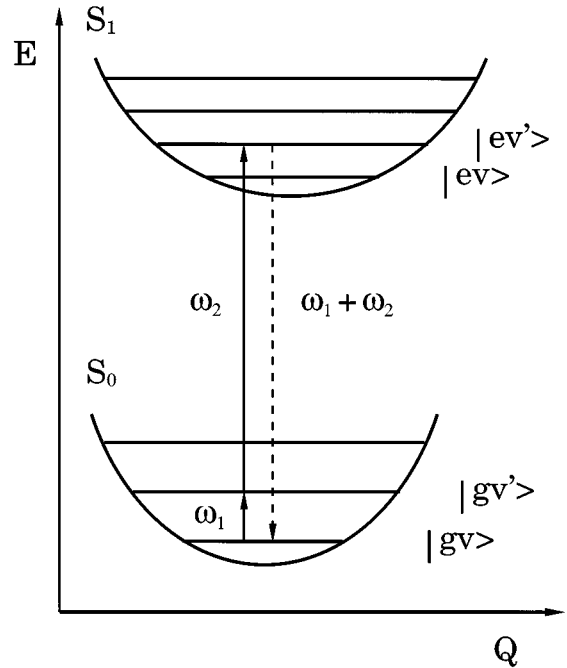


FIG. 1. Level scheme of interest in the study of DR IRVSFG process. The IR and visible transitions are represented, respectively, by the arrows labeled ω_1 and ω_2 . The frequency of the output signal is $\omega_1 + \omega_2$. The states $\{|gv\rangle\}$ and $\{|ev\rangle\}$ are, respectively, the vibronic states of the ground (S_0) and excited (S_1) potential energy surfaces.

where $L'_0 = L_0 - i\hbar\Gamma$. Here, L_0 denotes the Liouville operator for the free system. It is given by $L_0 = [H_0, \cdot]$, and is built on the molecular system Hamiltonian $H_0 = H_g |g\rangle\langle g| + H_e |e\rangle\langle e|$. The Hamiltonians of the ground and excited electronic configurations are taken in the harmonic approximation, i.e.,

$$H_g = \sum_f \hbar \omega_{g,f} (a_f^\dagger a_f + 1/2), \quad (2)$$

$$H_e = H_g + \hbar \omega_{eg} + \sum_f L_f A_f + \frac{1}{2} \sum_{ff'} V_{ff'} A_f A_{f'}, \quad (3)$$

where $A_f = i(a_f - a_f^\dagger)$, $\hbar \omega_{eg}$ is the electronic transition energy, and $\omega_{g,f}$ is the frequency of mode f in the ground electronic configuration. The coefficients L_f are related to the equilibrium position shifts for each mode in the linear coupling scheme while the quadratic vibronic coupling constants $V_{ff'}$ lead to frequency shifts and mode mixing as schematically shown in Figs. 1 and 2. It has been clearly established that the excited state normal coordinates represented by an N -dimensional vector \mathbf{d}_e are related to those of the ground state \mathbf{d}_g through the relation $\mathbf{d}_e = \mathbf{R}\mathbf{d}_g + \mathbf{\Delta}$ [7,19]. The matrix \mathbf{R} is an $N \times N$ orthogonal matrix ($\mathbf{R}\mathbf{R}^T = \mathbf{I}$) describing the Duschinsky rotation and the vector $\mathbf{\Delta}$ represents the overall equilibrium position displacement under electronic excitation for the general quadratic model. These quantities are related to the parameters \mathbf{L} and \mathbf{V} through the relations

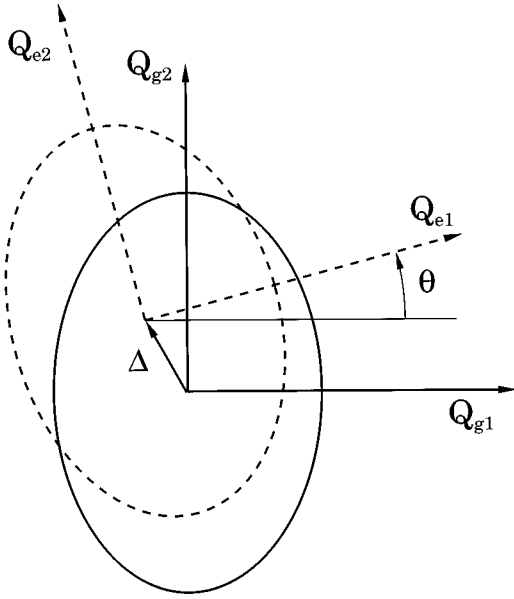


FIG. 2. Schematic representation of the equilibrium position shift and Duschinsky rotation under electronic excitation. In the case of a two-mode model depicted here, the normal coordinates $Q_{e,1}$ and $Q_{e,2}$ of the excited configuration are shifted by a vector Δ and rotated by an angle θ compared to the coordinates $Q_{g,1}$ and $Q_{g,2}$ of the ground electronic configuration.

$$\omega_e^2 = \mathbf{R}[\omega_g^2 + 2\hbar^{-1}\omega_g^{1/2}\mathbf{V}\omega_g^{1/2}]\bar{\mathbf{R}}, \quad \Delta = (2/\hbar)^{1/2}\omega_e^{-2}\mathbf{R}\omega_g^{1/2}\mathbf{L}. \quad (4)$$

Notice that ω_e and ω_g are $N \times N$ diagonal matrices made up of the frequencies of the vibrational modes, and \mathbf{R} is the orthogonal matrix which diagonalizes the expression $\omega_g^2 + 2\hbar^{-1}\omega_g^{1/2}\mathbf{V}\omega_g^{1/2}$. The other operators in Eq. (1) are Γ , the damping operator which takes into account the interactions between the system and its environment, and $L_v(t) = [V(t)]$, the Liouville operator for the system-radiation field interaction.

To get any information on the molecular system in an SFG experiment, the second order polarization is required. This quantity is defined as the mean value of the dipole moment, and can be written as

$$\mathbf{P}^{(2)}(t) = \text{Tr}\{\rho^{(2)}(t)\boldsymbol{\mu}\}. \quad (5)$$

Using a perturbation expansion, and with the introduction of the notation $\rho^\infty = \rho(-\infty)$ and $G_0(\tau) = \exp[-(i/\hbar)L'_0(\tau)]$, the

nondiagonal matrix elements of $\rho^{(2)}(t)$ are easily deduced, and the resulting polarization can be expressed as $\mathbf{P}^{(2)}(t) = \sum_{i=1}^2 \mathbf{P}_i^{(2)}(t) + \mathbf{P}_i^{(2)*}(t)$, where the various contributions correspond to

$$\begin{aligned} \mathbf{P}_1^{(2)}(t) = & -\frac{1}{\hbar^2} \sum_{g,k,l} \boldsymbol{\mu}_{gk} \rho_{gg}^\infty \int_{-\infty}^t d\tau_1 \int_{-\infty}^{\tau_1} d\tau_2 \\ & \times G_{0kgkg}(t-\tau_1) V(\tau_1)_{kl} G_{0lglg}(\tau_1-\tau_2) V(\tau_2)_{lg}, \end{aligned} \quad (6)$$

$$\begin{aligned} \mathbf{P}_2^{(2)}(t) = & \frac{1}{\hbar^2} \sum_{g,k,l} \boldsymbol{\mu}_{lk} \rho_{gg}^\infty \int_{-\infty}^t d\tau_1 \int_{-\infty}^{\tau_1} d\tau_2 \\ & \times G_{0klkl}(t-\tau_1) V(\tau_1)_{kg} G_{0glgl}(\tau_1-\tau_2) V(\tau_2)_{gl}. \end{aligned} \quad (7)$$

Usually, the initial density matrix $\rho_{gg}^\infty = \sum_g \mathcal{P}_g |g\rangle \langle g|$, corresponds to a Boltzmann distribution of vibrational states of the ground electronic configuration. In the dipole approximation, the operator $V(t)$ is given by the following expression:

$$V(t) = -\boldsymbol{\mu} \sum_{i=1}^2 \mathbf{E}_i(t),$$

$$\mathbf{E}_i(t) = [\mathcal{E}_i(\omega_i) e^{-i\omega_i t} + \mathcal{E}_i(-\omega_i) e^{i\omega_i t}], \quad (8)$$

where $\boldsymbol{\mu}$ is the dipole operator, the quantities $\mathbf{E}_1(t)$ and $\mathbf{E}_2(t)$, respectively, represent the infrared and the visible radiation field. Of course, the amplitudes of the field $\mathcal{E}_i(\omega_j)$ and $\mathcal{E}_j(-\omega_j)$ are related by complex conjugation, i.e., $\mathcal{E}_j(-\omega_j) = \mathcal{E}_j^*(\omega_j)$.

In the present calculation, we are interested in experiments where the infrared frequency is resonant with vibrational motions and where the visible frequency is resonant with electronic transitions as well. Consequently, only the contribution $\mathbf{P}_1^{(2)}(t)$ has to be taken into account. In an SFG experiment, only the terms which oscillate as $\exp[\pm i(\omega_i + \omega_j)t]$ contribute to the process. The terms with phase factor $\exp[\pm i(\omega_i - \omega_j)t]$ correspond to the difference frequency generation (DFG) process. If we take $\tau_2 = t - t_2 - t_1$ and $\tau_1 = t - t_1$, and if we perform the summation over the field subscripts, the second order contributions $\mathbf{P}_j^{(2)}(t)$, $j=1,2$ to the total polarization can be divided in two components $\mathbf{P}_{j,1}^{(2)}(t) + \mathbf{P}_{j,2}^{(2)}(t)$, which oscillate with the phase factor $\exp[-i(\omega_1 + \omega_2)t]$. They are given by the following quantities:

$$\begin{aligned} \mathbf{P}_{1,1(2)}^{(2)}(t) = & -\frac{1}{\hbar^2} \sum_{g,k,l} \boldsymbol{\mu}_{gk} (\boldsymbol{\mu}_{kl} \cdot \mathcal{E}_{2(1)}(\omega_{2(1)})) (\boldsymbol{\mu}_{lg} \cdot \mathcal{E}_{1(2)}(\omega_{1(2)})) \rho_{gg}^\infty \exp[-i(\omega_1 + \omega_2)t] \\ & \times \int_0^\infty dt_1 \int_0^\infty dt_2 \exp[-i(\omega'_{kg} - \omega_1 - \omega_2)t_1] \exp[-i(\omega'_{lg} - \omega_{1(2)})t_2], \end{aligned} \quad (9)$$

$$\begin{aligned} \mathbf{P}_{2,1(2)}^{(2)}(t) = & +\frac{1}{\hbar^2} \sum_{g,k,l} \boldsymbol{\mu}_{lk} (\boldsymbol{\mu}_{kg} \cdot \mathcal{E}_{2(1)}(\omega_{2(1)})) (\boldsymbol{\mu}_{gl} \cdot \mathcal{E}_{1(2)}(\omega_{1(2)})) \rho_{gg}^\infty \exp[-i(\omega_1 + \omega_2)t] \\ & \times \int_0^\infty dt_1 \int_0^\infty dt_2 \exp[-i(\omega'_{kl} - \omega_1 - \omega_2)t_1] \exp[-i(\omega'_{gl} - \omega_{1(2)})t_2]. \end{aligned} \quad (10)$$

These expressions correspond, respectively, to the case where the system interacts first with the field at frequency ω_1 (ω_2), then with the second field at frequency ω_2 (ω_1). Notice that we have neglected the contributions which are nonresonant assuming that the frequencies ω_1 and ω_2 are defined positive.

In the following, we consider two electronic configurations with their corresponding vibrational states. The vibronic states which belong to the ground electronic configuration are denoted $|gv\rangle$ and $|gv'\rangle$, while those corresponding to the excited electronic configuration are labeled $|ev'\rangle$ and $|ev''\rangle$. Hence, the states involved in resonant contributions to $\mathbf{P}_{j,1}^{(2)}(t)$ correspond to $|g\rangle \rightarrow |gv\rangle$, $|l\rangle \rightarrow |gv'\rangle$, $|k\rangle \rightarrow |ev''\rangle$, and those participating in $\mathbf{P}_{j,2}^{(2)}(t)$ are given by $|g\rangle \rightarrow |gv\rangle$, $|l\rangle \rightarrow |ev'\rangle$, $|k\rangle \rightarrow |ev''\rangle$. We further consider that the electronic dephasing constants $\Gamma_{ev'gv} = \Gamma_{eg}$ and the vibrational dephasing constant $\Gamma_{iv'iv} = \gamma_i$ for $i = \{e, g\}$. From the time scales typical of molecular dynamics, we also introduce the approximation $\gamma_i \ll \Gamma_{eg}$. In this limit, $\mathbf{P}_{j,2}^{(2)}(t)$ can be neglected before $\mathbf{P}_{j,1}^{(2)} \times(t)$. Consequently, the second order polarization reduces to the case where the infrared field interacts first with the molecule. Next, we introduce the components of the second order susceptibility defined by the expression

$$P_{jx}^{(2)}(t) = \sum_{y,z} \chi_{j1}^{(2)}(\omega_{sf})_{xyz} \mathcal{E}_{1y}(\omega_1) \mathcal{E}_{2z}(\omega_2) \exp[-i(\omega_{sf})t], \quad (11)$$

for $j=1, 2$, and where $\omega_{sf} = \omega_1 + \omega_2$. The third rank tensor components can easily be deduced by the use of Eq. (9) and Eq. (11). For $v' \neq v$, they can be written as

$$\begin{aligned} \chi_{11}^{(2)}(\omega_{sf})_{xyz} = & -\frac{1}{\hbar^2} \sum_{v,v',v''} \mathcal{F}_1^{xyz} \rho_{gvgv}^\infty \int_0^\infty dt_1 \int_0^\infty dt_2 \\ & \times e^{-i(\omega_{ev''gv} - i\Gamma_{eg} - \omega_{sf})t_1 - i(\omega_{gv'gv} - i\gamma_g - \omega_1)t_2}, \end{aligned} \quad (12)$$

$$\begin{aligned} \chi_{21}^{(2)}(\omega_{sf})_{xyz} = & +\frac{1}{\hbar^2} \sum_{v,v',v''} \mathcal{F}_2^{xyz} \rho_{gvgv}^\infty \int_0^\infty dt_1 \int_0^\infty dt_2 \\ & \times e^{-i(\omega_{gv'ev''} - i\Gamma_{eg} - \omega_{sf})t_1 - i(\omega_{gv'gv} - i\gamma_g - \omega_1)t_2}, \end{aligned} \quad (13)$$

where we have introduced the following notation: $\mathcal{F}_1^{xyz} = \mu_{gvev''}^x \mu_{ev''gv'}^y \mu_{gv'gv}^z$ and $\mathcal{F}_2^{xyz} = \mu_{ev''gv'}^x \mu_{gvev''}^y \mu_{gv'gv}^z$.

The evaluation of the vibronic dipole moment matrix elements in Eq. (12) and Eq. (13) can be simplified by introducing a Born-Oppenheimer state representation based on the adiabatic approximation. In this case, we have

$$\mu_{fv'iv} = \langle \Psi_{fv'} | \boldsymbol{\mu} | \Psi_{iv} \rangle = \langle \Theta_{fv'} | \boldsymbol{\mu}_{fi} | \Theta_{iv} \rangle, \quad (14)$$

where the molecular states $|\Psi_{iv}\rangle = |\Phi_i \Theta_{iv}\rangle$ and $|\Psi_{fv'}\rangle = |\Phi_{f'} \Theta_{fv'}\rangle$ are, respectively, the products of the electronic and vibrational wave functions of the initial and final states. Consequently, Eq. (12) and Eq. (13) reduce to

$$\begin{aligned} \chi_{11}^{(2)}(\omega_{sf})_{xyz} = & -\frac{1}{\hbar^2} \int_0^\infty dt \int_0^\infty dt' e^{i(\omega_{sf} + i\Gamma_{eg})t} e^{i(\omega_1 + i\gamma_g)t'} \\ & \times \langle e^{itH_g/\hbar} \mu_{ge}^x e^{-itH_e/\hbar} \mu_{eg}^y e^{-it'H_g/\hbar} \\ & \times \mu_{gg}^z e^{it'H_g/\hbar} \rangle, \end{aligned} \quad (15)$$

$$\begin{aligned} \chi_{21}^{(2)}(\omega_{sf})_{xyz} = & +\frac{1}{\hbar^2} \int_0^\infty dt \int_0^\infty dt' e^{i(\omega_{sf} + i\Gamma_{eg})t} e^{i(\omega_1 + i\gamma_g)t'} \\ & \times \langle e^{-it'H_g/\hbar} \mu_{gg}^z e^{itH_g/\hbar} e^{it'H_g/\hbar} \mu_{ge}^x \\ & \times e^{-itH_e/\hbar} \mu_{eg}^y \rangle, \end{aligned} \quad (16)$$

where H_g and H_e are, respectively, the Hamiltonians of the ground and excited electronic configuration, and where $\langle O \rangle = \text{Tr}\{O e^{-\beta H_g}\} / \text{Tr}\{e^{-\beta H_g}\}$ denotes the thermal average of an operator O . We also defined the SFG time correlators $C_{eg}^1(t, t')$ and $C_{eg}^2(t, t')$ by

$$\begin{aligned} C_{eg}^1(t, t') = & \langle e^{itH_g/\hbar} \mu_{ge}^x e^{-itH_e/\hbar} \mu_{eg}^y e^{-it'H_g/\hbar} \mu_{gg}^z e^{it'H_g/\hbar} \rangle \\ = & \langle \tilde{\mu}_{ge}^x(t) S^+(t) \tilde{\mu}_{eg}^y(0) \tilde{\mu}_{gg}^z(-t') \rangle, \end{aligned} \quad (17)$$

$$\begin{aligned} C_{eg}^2(t, t') = & \langle e^{-it'H_g/\hbar} \mu_{gg}^z e^{itH_g/\hbar} e^{it'H_g/\hbar} \mu_{ge}^x e^{-itH_e/\hbar} \mu_{eg}^y \rangle \\ = & \langle \tilde{\mu}_{gg}^z(-t') \tilde{\mu}_{ge}^x(t) S^+(t) \tilde{\mu}_{eg}^y(0) \rangle, \end{aligned} \quad (18)$$

where the operators $S^+(t)$ and $\tilde{\mu}(t)$ are defined by

$$S^+(t) = e^{itH_g/\hbar} e^{-itH_e/\hbar}, \quad \tilde{\mu}(t) = e^{itH_g/\hbar} \boldsymbol{\mu} e^{-itH_g/\hbar}. \quad (19)$$

In these equations, $\tilde{\mu}(t)$ is the dipole moment evaluated in the interaction picture at time t , and the thermal average $\langle S^+(t) \rangle$ of the operator $S^+(t)$ is the basic quantity used in the calculation of the optical absorption of a molecular system [13–16, 19, 29–31].

Moreover, if the vibrational dipole moments $\boldsymbol{\mu}_{gg}$, as well as the electronic dipole moments $\boldsymbol{\mu}_{eg}$, depend weakly on the vibrational coordinate $Q_f = i\sqrt{2}\omega_{gf}/\hbar(a_f - a_f^+)$ for the mode f , we expand the transition moments as [2, 16]

$$\begin{aligned} \boldsymbol{\mu}_{kl} = & \boldsymbol{\mu}_{kl}(0) + \sum_f \left(\frac{\partial \boldsymbol{\mu}_{kl}}{\partial Q_f} \right)_0 Q_f \\ & + \frac{1}{2} \sum_{f,f'} \left(\frac{\partial^2 \boldsymbol{\mu}_{kl}}{\partial Q_f \partial Q_{f'}} \right)_0 Q_f Q_{f'} + \dots \end{aligned} \quad (20)$$

In the Condon approximation, only the first term $\boldsymbol{\mu}_{kl}(0)$ of Eq. (20) is kept. This term vanishes for a transition between vibrational states. For our purpose, we only consider the second term of Eq. (20) for vibrational transition, and only the first one in the case of an electronic transition [2]. The dipolar transition moments are given by

$$\mu_{eg}^x = \mu_{eg}^x(0), \quad \mu_{gg}^z = \mu_{gg}^z(0) \left(1 + \sum_f m_f^z \mathcal{A}_f \right), \quad (21)$$

and the SFG time correlators reduce to

$$C_{eg}^1(t, t') = \mu_{ge}^x(0) \mu_{eg}^y(0) \langle S^+(t) \tilde{\mu}_{gg}^z(-t') \rangle, \quad (22)$$

$$C_{eg}^2(t, t') = \mu_{ge}^x(0) \mu_{eg}^y(0) \langle \tilde{\mu}_{gg}^z(-t') S^+(t) \rangle. \quad (23)$$

To evaluate these expressions, we consider the functions $C_{eg}^1(\lambda, t, t')$ and $C_{eg}^2(\lambda, t, t')$ defined by

$$C_{eg}^1(\lambda, t, t') = \mathcal{M}_{ge}^{xyz} \left\langle S^+(t) \exp \left(\lambda \sum_f m_f^z \mathcal{A}_f(-t') \right) \right\rangle, \quad (24)$$

$$C_{eg}^2(\lambda, t, t') = \mathcal{M}_{ge}^{xyz} \left\langle \exp \left(\lambda \sum_f m_f^z \mathcal{A}_f(-t') \right) S^+(t) \right\rangle, \quad (25)$$

where the parameter λ has been introduced and $\mathcal{M}_{ge}^{xyz} = \mu_{ge}^x(0) \mu_{eg}^y(0) \mu_{gg}^z(0)$. If we expand $C_{eg}^j(\lambda, t, t')$ in first-order Taylor series, neglect the zero-order term, and set λ equal to 1, the SFG time correlator $C_{eg}^j(t, t')$ is recovered [16].

III. DIAGRAMMATIC EXPANSION

This section is devoted to the evaluation of the functions $C_{eg}^j(\lambda, t, t')$ by a diagrammatic expansion of the corresponding time correlator. To this end, the generalization of Wick's theorem introduced by Page and Tonks [13], as well as a diagrammatic expansion similar to the one used in their calculation of the Raman time correlator $A(t', t, \mu)$, will be employed [13, 19, 29]. The operator $S^+(t)$ can be expressed as a time-ordered exponential

$$S^+(t) = T_+ \exp \left[-i/\hbar \int_0^t d\tau V_{eg}(\tau) \right], \quad (26)$$

where $V_{eg}(\tau)$ is the difference between the excited state and the ground state Hamiltonians taken in the interaction picture. The time ordering operator T_+ places the operators of later times to the left of those of earlier times [29], and the time correlators $C_{eg}^j(\lambda, t, t')$ can be written as

$$C_{eg}^1(\lambda, t, t') = \mathcal{M}_{ge}^{xyz} \exp[-i\omega_{eg}t] \langle T_{tt'} \exp \Phi \rangle, \quad (27)$$

$$C_{eg}^2(\lambda, t, t') = \mathcal{M}_{ge}^{xyz} \exp[-i\omega_{eg}t] \langle T_{t't} \exp \Phi \rangle, \quad (28)$$

where $T_{tt'}$ is a generalized time-ordering operator which keeps operators involving unprimed time evolution to the left of those involving primed time evolution. Moreover, this time-ordering operator orders unprimed $V_{eg}(\tau)$ with T_+ . The additional quantity Φ is defined as

$$\Phi = \lambda \sum_f m_f^z \mathcal{A}_f(-t') - \frac{i}{\hbar} \int_0^t d\tau \left(\sum_f L_f \mathcal{A}_f(\tau) + \frac{1}{2} \sum_{ff'} V_{ff'} \mathcal{A}_f(\tau) \mathcal{A}_{f'}(\tau) \right). \quad (29)$$

The time-ordered thermal average factor in Eq. (27) can be developed in Taylor series, and takes the form $\langle T_{tt'} \exp \Phi \rangle = \sum_k \langle T_{tt'} \Phi^k \rangle / k!$. The application of the generalized Wick's theorem introduced in Appendix B of [13] allows us to reduce $\langle T_{tt'} \Phi^k \rangle$ to a product of thermally averaged time-ordered pairs.

The diagrammatic representation of $\langle T_{tt'} \Phi^k \rangle$ is quite similar to the one used by Tonks and Page in [19, 29]. The linear electron-vibration interaction vector $-i/\hbar \mathbf{L}$ and the quadratic vibronic mode coupling matrix $-i/2\hbar \mathbf{V}$ are, respectively, represented by dot and circle vertices with $-$ signs. The linear vector $\lambda \mathbf{m}$, which lists the first-order non-Condon dipole moment coefficients, is simply depicted by a dot vertex surmounted by a (\star) . The time-ordered thermal average in Eq. (27) reduces to

$$\langle T_{tt'} \exp \Phi \rangle = \exp \sum_k \langle T_{tt'} \Phi^k \rangle_l / k!, \quad (30)$$

where the subscript l refers to the ‘‘linked’’ diagrams in the pictorial representation of $\langle T_{tt'} \Phi^k \rangle$. If a supplementary factor 2 is incorporated in the matrix $-(i/2\hbar) \mathbf{V}$, the mean value $\langle T_{tt'} \Phi^k \rangle_l / k!$ reduces to the following diagrammatic expressions:

$$\begin{aligned} \langle T_{tt'} \Phi_1 \rangle / 1! &= \frac{1}{2} \left[\text{---} \ominus \text{---} \right], \\ \langle T_{tt'} \Phi_2 \rangle / 2! &= \frac{1}{2} \left[\text{---} \ominus \text{---} + \frac{1}{2} \left(\text{---} \ominus \ominus \text{---} \right) + 2 \left(\star \text{---} \ominus \text{---} \right) \right], \\ \langle T_{tt'} \Phi_3 \rangle / 3! &= \frac{1}{2} \left[\text{---} \ominus \ominus \text{---} + \frac{1}{3} \left(\text{---} \ominus \ominus \ominus \text{---} \right) + 2 \left(\star \text{---} \ominus \text{---} \right) \right], \\ \langle T_{tt'} \Phi_n \rangle / n! &= \frac{1}{2} \left[\text{---} \ominus \text{---} \cdots \text{---} \ominus \text{---} + \frac{1}{n} \left(\text{---} \ominus \cdots \ominus \text{---} \right) + 2 \left(\star \text{---} \ominus \text{---} \right) \right]. \end{aligned} \quad (31)$$

In [18, 19, 29], Tonks and Page have derived analytical expressions for the sum of diagrams with $-$ vertices only, as well as for their complex conjugates involving $+$ vertices. They have defined two functions $F_c(t)$ and $F_d(t)$, whose pictorial representation is given by

$$F_c(t) = \frac{1}{2} \left[\text{---} \ominus \text{---} + \frac{1}{2} \left(\text{---} \ominus \ominus \text{---} \right) + \frac{1}{3} \left(\text{---} \ominus \ominus \ominus \text{---} \right) + \cdots + \frac{1}{n} \left(\text{---} \ominus \cdots \ominus \text{---} \right) \right], \quad (32)$$

$$F_d(t) = \frac{1}{2} \left[\text{---} \ominus \text{---} + \text{---} \ominus \text{---} \text{---} + \cdots + \text{---} \ominus \text{---} \cdots \text{---} \text{---} \right]. \quad (33)$$

The algebraic forms of these functions reduce to

$$F_d(t) = \frac{1}{2} \sum_{f_1 f_2} \int_0^t dt_1 \int_0^t dt_2 (-i/\hbar L_{f_1}) S_{f_1 f_2}(t, t_1, t_2) \times (-i/\hbar L_{f_2}), \quad (34)$$

$$F_c(t) = \frac{1}{2} \sum_{f_1 f_2} \int_0^t dt_1 S_{f_1 f_2}(t_1, t_1, t_1) (-i/\hbar V_{f_2 f_1}). \quad (35)$$

In the description of RRS experiments, the Raman time-correlator $A(t', t, \mu)$ is defined by

$$A(t', t, \mu) = \langle \exp(it' H_e / \hbar) \exp(i\mu H_g / \hbar) \times \exp(-it H_e / \hbar) \exp[i(\mu + t' - t) H_g / \hbar] \rangle. \quad (36)$$

There is a close connection between Raman and optical absorption correlators [29]. This relation is given by

$$A(t', t, \mu) = \eta^*(t') \eta(t) \exp \sum_{k=1}^{\infty} \gamma_k(t, t', \mu), \quad (37)$$

where the absorption time correlator $\eta(t)$ is written as

$$\eta(t) = \exp[-i\omega_e t] \langle T_+ \exp \Phi \rangle = \exp[-i\omega_e t + F_d(t) + F_c(t)]. \quad (38)$$

This function can be calculated exactly with the help of Eq. (34). Unfortunately, the Raman time-correlator itself cannot be handled as easily because of the term $\exp \sum_k \gamma_k(t, t', \mu)$ in Eq. (37). But it is possible to separate the RRS into orders. The n th order scattering is given by the summation of all the terms $\Pi \gamma_k(t, t', \mu)$ in the Taylor's series expansion of the preceding exponential, with the condition $\sum k = n$. At $T=0$ K, the n th order scattering corresponds to the total intensity of all n -phonon Stokes lines [29].

In the case of the SFG time correlator [2,20], on the other hand, it is straightforward to show that the functions $C_{eg}^j(\lambda, t, t')$ can be factorized into products of a function $\exp \psi_j(\lambda, t, t')$ by the absorption time correlator $\eta(t)$, namely,

$$C_{eg}^j(\lambda, t, t') = \mathcal{M}_{ge}^{xyz} \eta(t) \exp \psi_j(\lambda, t, t'). \quad (39)$$

Notice that this expression can be evaluated exactly since the function $\psi_1(\lambda, t, t')$ is defined by the following diagrams:

$$\psi_1(\lambda, t, t') = \left[\begin{array}{c} \overline{\bullet} \text{---} \star + \overline{\bullet} \text{---} \ominus \text{---} \star + \dots \\ + \overline{\bullet} \text{---} \ominus \text{---} \dots \text{---} \ominus \text{---} \star \end{array} \right], \quad (40)$$

and takes the algebraic form

$$\psi_1(\lambda, t, t') = \lambda \sum_{f_1} m_{f_1}^z \int_0^t dt_1 \kappa_{f_1}(t, t_1) h_{f_1}(t_1 + t'), \quad (41)$$

with the vectorial function $\kappa(t, t_1)$ defined by

$$\kappa_{f_1}(t, t_1) = (-i/\hbar L_{f_1}) + \sum_{f_2 f_3} \int_0^t dt_2 \times (-i/\hbar V_{f_1 f_2}) S_{f_2 f_3}(t, t_1, t_2) (-i/\hbar L_{f_3}). \quad (42)$$

In Eqs. (34) and (42), the function $S_{f_1 f_2}(t, t_1, t_2)$ is the solution to a Dyson-like equation whose analytical expression has been derived in [18,19,29].

The scalar functions $F_c(t)$ and $F_d(t)$ are given by

$$F_c(t) = \frac{1}{2} it \text{Tr} \boldsymbol{\omega}^- + N \ln 2 + \frac{1}{2} \ln(\det\{\boldsymbol{\omega}_g \boldsymbol{\omega}_e [I - \boldsymbol{\Gamma}^{-1}(0)]^2\}) + \frac{1}{2} \ln(\det\{-\mathbf{f}^+(t) \mathbf{f}^-(t)\}), \quad (43)$$

$$F_d(t) = \frac{1}{2} it \tilde{\mathbf{L}}'' \boldsymbol{\omega}_g^3 \boldsymbol{\omega}_e^{-2} \mathbf{L}'' - \tilde{\mathbf{L}}'' \boldsymbol{\omega}_g^{3/2} \boldsymbol{\omega}_e^{-2} \mathbf{R} \boldsymbol{\omega}_g \tilde{\mathbf{R}} [\boldsymbol{\Gamma}^{-1}(t) - I] \times \mathbf{f}^+(t) [I - \boldsymbol{\theta}(-t)] \boldsymbol{\omega}_e^{-1} \boldsymbol{\omega}_g^{3/2} \mathbf{L}'', \quad (44)$$

where the following simplifying notations have been introduced [16]:

$$\mathbf{f}^{\pm}(t) = \{[\boldsymbol{\omega}^- \pm \boldsymbol{\theta}(-t) \boldsymbol{\omega}^+] \boldsymbol{\Gamma}^{-1}(t) - [\boldsymbol{\theta}(-t) \boldsymbol{\omega}^- \pm \boldsymbol{\omega}^+]\}^{-1}, \quad (45)$$

$$\mathbf{L}'' = 2^{1/2} \boldsymbol{\omega}_g^{-3/2} \mathbf{R} \boldsymbol{\omega}_g^{3/2} \boldsymbol{\xi}, \quad \boldsymbol{\xi} = (\hbar \boldsymbol{\omega}_g)^{-1} \mathbf{L}, \quad \boldsymbol{\omega}^{\pm} = \mathbf{R} \boldsymbol{\omega}_g \tilde{\mathbf{R}} \pm \boldsymbol{\omega}_e, \quad (46)$$

$$\boldsymbol{\Gamma}^{-1}(t) = \exp[(-\beta \hbar + it) \mathbf{R} \boldsymbol{\omega}_g \tilde{\mathbf{R}}], \quad \boldsymbol{\theta}(t) = \exp(it \boldsymbol{\omega}_e). \quad (47)$$

An algebraic form for Eq. (41) can be obtained similarly. It is given by the following closed-form expressions:

$$\psi_1(\lambda, t, t') = \lambda \sqrt{2\tilde{m}^z} \boldsymbol{\omega}_g^{1/2} \tilde{\mathbf{R}} [\boldsymbol{\chi}(t') \boldsymbol{\Gamma}^{-1}(t) + \boldsymbol{\chi}(-t')] \times \mathbf{f}^+(t) [I - \boldsymbol{\theta}(-t)] \boldsymbol{\omega}_e^{-1} \boldsymbol{\omega}_g^{3/2} \mathbf{L}'', \quad (48)$$

$$\psi_2(\lambda, t, t') = \lambda \sqrt{2\tilde{m}^z} \boldsymbol{\omega}_g^{1/2} \tilde{\mathbf{R}} [\boldsymbol{\chi}(t') \boldsymbol{\chi}(-i\beta \hbar) \boldsymbol{\Gamma}^{-1}(t) + \boldsymbol{\chi}(-t') \boldsymbol{\chi}(i\beta \hbar)] \mathbf{f}^+(t) \times [I - \boldsymbol{\theta}(-t)] \boldsymbol{\omega}_e^{-1} \boldsymbol{\omega}_g^{3/2} \mathbf{L}'', \quad (49)$$

$$\boldsymbol{\chi}(t') = \exp(it' \mathbf{R} \boldsymbol{\omega}_g \tilde{\mathbf{R}}). \quad (50)$$

As stated in the preceding section, the SFG time correlator is obtained from the first order term of the Taylor expansion of the function $C_{eg}^j(\lambda, t, t')$, setting $\lambda = 1$. Thus we have

$$C_{eg}^j(t, t') = \mathcal{M}_{ge}^{xyz} \psi_j(1, t, t') \eta(t). \quad (51)$$

In the approximation of molecular systems with general harmonic potential surfaces, this function gives an exact analytical expression for the time correlator needed to calculate the SFG susceptibility of adsorbed molecules $\chi^{(2)}(\boldsymbol{\omega}_{sf})_{xyz} = \chi_{11}^{(2)}(\boldsymbol{\omega}_{sf})_{xyz} + \chi_{21}^{(2)}(\boldsymbol{\omega}_{sf})_{xyz}$,

$$\chi^{(2)}(\omega_{sf})_{xyz} = -\frac{\mathcal{M}_{ge}^{xyz}}{\hbar^2} \int_0^\infty dt [\Psi_1(t) - \Psi_2(t)] \times \exp[i\Delta\omega t - \Gamma_{eg}t + F_d(t) + F_c(t)], \quad (52)$$

where $\Delta\omega = \omega_1 + \omega_2 - \omega_{eg}$, and the time dependent functions $\Psi_{1(2)}(t)$ are given by the following closed formulas :

$$\begin{aligned} \Psi_j(t) = & i\sqrt{2\tilde{m}^z} \omega_g^{1/2} [(\omega_1 - \omega_g + i\gamma_g)^{-1} \tilde{\mathbf{R}}\boldsymbol{\gamma}(i\beta\hbar(j-1)) \\ & + (\omega_1 + \omega_g + i\gamma_g)^{-1} \tilde{\mathbf{R}}\boldsymbol{\gamma}(-i\beta\hbar(j-1)) \Gamma^{-1}(t)] \\ & \times f^+(t) [I - \boldsymbol{\theta}(-t)] \omega_e^{-1} \omega_g^{3/2} \mathbf{L}'''. \end{aligned} \quad (53)$$

Of course, if we set $\mathbf{R}=\mathbf{I}$ and $\omega_e = \omega_g$, i.e., take the limit of no mode-mixing and no frequency-shift for DR IVSFG, the results of the model by Huang and Shen [2] are easily recovered.

Thus we have established the expressions needed to proceed to the numerical study of the DR IVSFG spectra. Our model is valid for any given temperature and for an arbitrary number of active vibrational modes. Let us mention at this point that the main advantage of the diagrammatic theory used here is the simplicity of the analytical expressions which are easy to program on a computer. Though this approach may seem more abstract than the standard sum-over-state method with its overlap integrals and energy denominators, it really is compendious. Indeed, for the DR IVSFG process, it is possible to sum over all the diagrams, thus obtaining analytical expressions which are exact, whereas for RRS, in the presence of mode mixing, some contributions have to be neglected leading to approximate results. Notice that in the absence of Duschinsky rotation, i.e., $\mathbf{R}=\mathbf{I}$ but $\omega_e \neq \omega_g$, the sum-over-state method also leads to an exact result for RRS [22,32].

IV. NUMERICAL SIMULATIONS AND DISCUSSIONS

To illustrate the basic features of SFG spectra as predicted by our theoretical model, we consider a molecule having only two electronic states with an energy gap $\hbar\omega_{eg}$ of 20 000 cm^{-1} , as well as only two vibrational modes. An electronic transition dipole moment, that need not be specified numerically here, couples the system with the visible excitation field while the modulations of the ground state permanent dipole moment by the vibrations of the molecule $(\partial\boldsymbol{\mu}_{gg}/\partial Q_f)_0$, assumed identical for both modes in the following, will make them absorb infrared light. When the molecule is in its ground electronic state, the frequencies of the vibrational modes have been chosen as 500 cm^{-1} and 800 cm^{-1} , whereas in the excited state they change slightly to 520 cm^{-1} and 790 cm^{-1} . In addition, the excited state potential well equilibrium position is shifted with respect to the ground state's and its principal axes are rotated as schematically shown in Fig. 2. It is further assumed that the experiment is being carried out at room temperature, i.e., $kT=200 \text{ cm}^{-1}$, so that only the ground vibrational state is predominantly populated before the external excitations are switched on. Finally, the damping constants setting the linewidths in the spectra have been chosen as follows: the

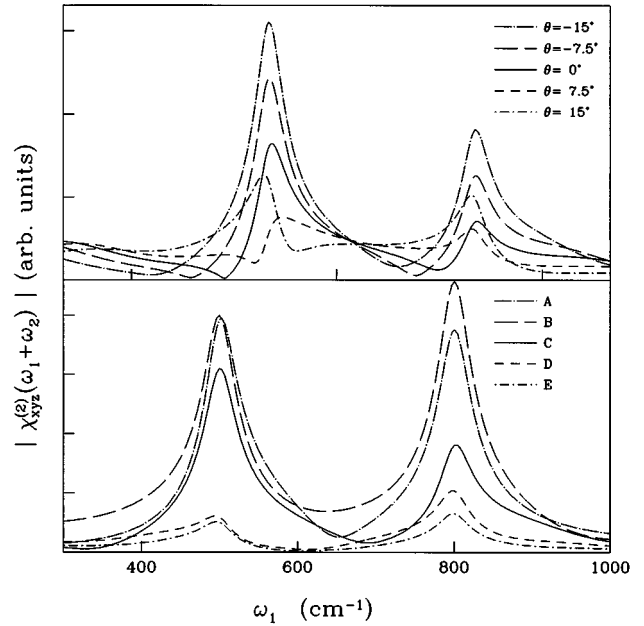


FIG. 3. SFG spectra vs the infrared frequency ω_1 for different values of the mode mixing angle θ in the upper half, and for different visible frequencies ω_2 , with $\theta = -15^\circ$, in the lower half. The labels A to E correspond to increasing values of ω_2 from 19 000 cm^{-1} to 21 000 cm^{-1} by steps of 500 cm^{-1} . Other parameters as indicated in the text.

electronic dephasing constant $\Gamma_{eg}=90 \text{ cm}^{-1}$, and the vibrational dephasing constants $\gamma_i=20 \text{ cm}^{-1}$. Before we present our results, we need to point out that the SFG spectra have been computed assuming parallel polarizations for the infrared and visible fields.

It is convenient to start our presentation of the numerical simulations with spectra which are drawn as a function of the frequency of the infrared excitation. In the case where the excitation in the visible range is far from any resonance, one can imagine the SFG experiment as infrared spectroscopy with a built-in up-conversion scheme making it possible to detect the signal in the visible range. However, when the experiment is being carried out so that an electronic absorption band is excited resonantly, the DR IVSFG process probes the excited state potential well as we shall see.

While the aforementioned parameters are being held fixed, we present in Fig. 3 the results obtained for different values of the Duschinsky rotation angle θ as well as those for the fixed angle of -15° but for increasing wave numbers of the visible excitation from 19 000 cm^{-1} to 21 000 cm^{-1} by increments of 500 cm^{-1} . The dimensionless displacements of the vibrational modes have been arbitrarily set to 0.5 in this plot.

Examining the upper half of Fig. 3, we notice that the mixing between modes results in marked distortions of the resonances along with some changes in relative intensities of the peaks. While all five curves seem to cross each other at about the same point close to the center of the plot, the sharpness of this feature depends on the exact value of the parameters, but furthermore, it is specific to the two-mode model. In the lower half of Fig. 3, we show that the exact value of the frequency of the visible excitation strongly af-

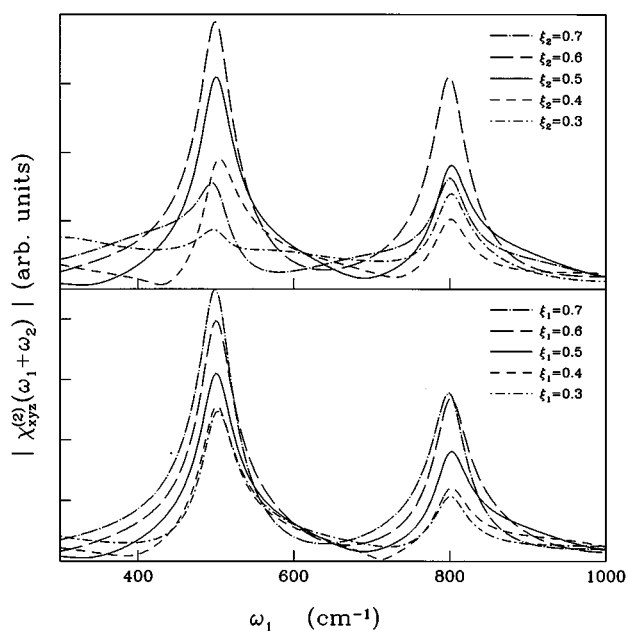


FIG. 4. SFG spectra vs the infrared frequency for different values of the displacements. In the upper half $\xi_2=0.5$ is fixed while ξ_1 varies. In the lower half $\xi_1=0.5$. The other parameters are identical to those of Fig. 3.

fects the overall intensity of the signal as well as the relative heights of the peaks but alters the shape of the spectra to a much lesser extent.

In Fig. 4, we represent the alternate situation where the amount of mode mixing is held constant while the mode displacements take different values. We see that, depending on the mode being displaced, the line shapes may or may not change while the intensities of the two resonances vary on a scale comparable to that of the previous figure.

Let us first mention that the asymmetric line shapes shown in the upper halves of Figs. 3 and 4 qualitatively look very much like those determined experimentally by Shen *et al.* [33] in the first observation of such an SFG vibrational spectrum. In that experiment, the visible excitation was sufficiently close to the shoulder of the visible absorption band that some resonance enhancement helped in strengthening the signal. The second point that we wish to make is that the interpretation of Raman scattering data [10,15,16] as well as the result from quantum chemistry computations [8,15,34] seem to indicate that Duschinsky rotation angles of up to 15° are not uncommon. In addition, the reduced equilibrium position displacements used here are rather normal as well. Yet our study shows that both parameters may have comparable effects. Hence, albeit the second order vibronic coupling is smaller than the linear term, it may alter the DR IVSFG spectra to a comparable, if not larger, extent.

Instead of recording DR IRVSFG spectra with respect to the frequency of the infrared source, one may choose to keep it close to a vibrational resonance and to record spectra with respect to the wavelength of the visible excitation. This is the experiment being simulated in Figs. 5 and 6 where we present again spectra for various values of the mode mixing angle and the dimensionless displacement of the lower frequency mode.

Each figure consists of two parts, the upper half showing

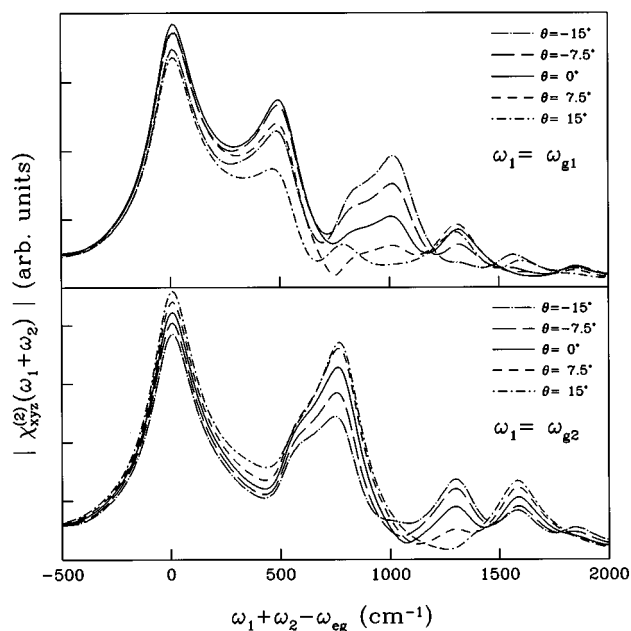


FIG. 5. SFG spectra vs the detuning of the visible excitation for various values of the mode mixing angle θ . The infrared excitation is resonant with $\omega_{g,1}$ transition in the upper half, and with the $\omega_{g,2}$ transition in the lower half.

the case where the infrared source resonantly excites the first vibrational mode while in the lower half it excites the second mode. Notice that we have chosen to plot the spectra versus a linear function of the wave number of the visible excitation, and not ω_2 itself, since we are really performing some sort of vibrational spectroscopy. Here, ω_{eg} denotes the electronic energy and not the vertical transition energy, so that

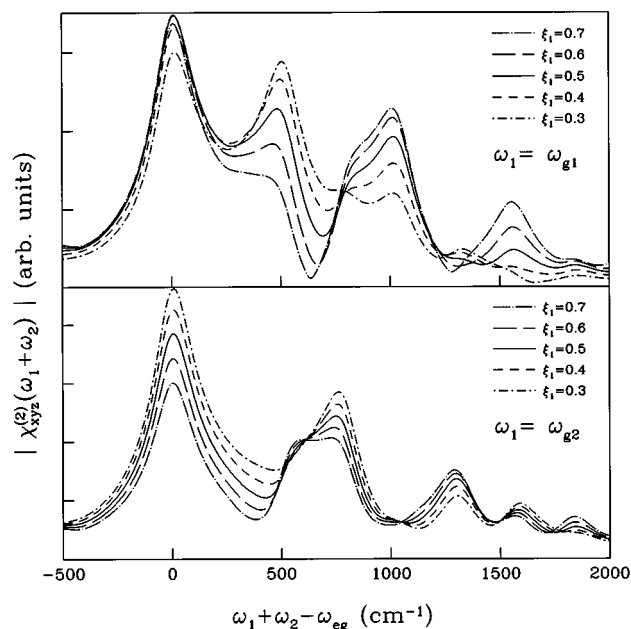


FIG. 6. SFG spectra vs the detuning of the visible excitation for various values of the 520 cm^{-1} mode displacement ξ_1 . The displacement of the 790 cm^{-1} mode $\xi_2=0.5$, and the Duschinsky angle $\theta=-15^\circ$. Infrared excitation as in Fig. 5.

TABLE I. The parameters used in our simulations are given here. The values which correspond to the first and the second normal mode are given in the form $\text{mode}_1|\text{mode}_2$, the vectors ξ and \tilde{m}^z are dimensionless.

	$\omega_{g,f}$ (cm^{-1})	ξ	\tilde{m}^z	$\omega_{e,f}$ (cm^{-1})	θ (degrees)
I	500 800	0.5 0.5	0.1 0.1	520 790	-15
II	518.9 773.1	0.723 0.399		518.9 773.1	0
III	498.9 799.5	0.618 0.503	0.109 0.098	498.9 799.5	0
IV	515.8 701.2	0.725 0.434	0.116 -0.274	515.8 701.2	0

the position of the various features are not affected by the parameters, making the figure easier to read.

The origin of the axis represents the sum frequency corresponding to the $0-0$ transition, the infrared excitation creating one quantum of vibration in one of the modes while the visible source is resonant with the $1-0$ transition for that mode. As ω_2 increases from there, the spectra display resonant features every time we sweep over a specific vibronic transition involving one or both modes.

In addition, between adjacent resonances the contributions of two vibronic transitions may interfere, leading to sharp dips in the spectrum like the one observed in the upper half of Fig. 6. Hence, this type of experiment results in much richer spectra than those discussed previously. But we see again that both the quadratic and the linear coupling terms, i.e., the mode mixing and the displacements, affect the spectra to the same extent, if not in the exact same way.

From the previous observations, it follows that we need to address the problem of discriminating between linear and quadratic effects when interpreting experimental spectra. In the field of Raman spectroscopy, one can take advantage of a relation between the optical absorption and the Raman spectra which holds when the coupling is linear, to identify the situations where one needs to include quadratic terms in the model. Unfortunately, this is not the case here and therefore we cannot trust a model based on equilibrium position shifts alone to interpret experimental data.

To illustrate this point, we have performed a series of least square fits with the linear model of the results for the optical absorption and both types of DR IRVSFG spectroscopies obtained for our model system with both linear and quadratic parameters. The reference parameters are those listed as entry I of Table I. They include the frequencies of

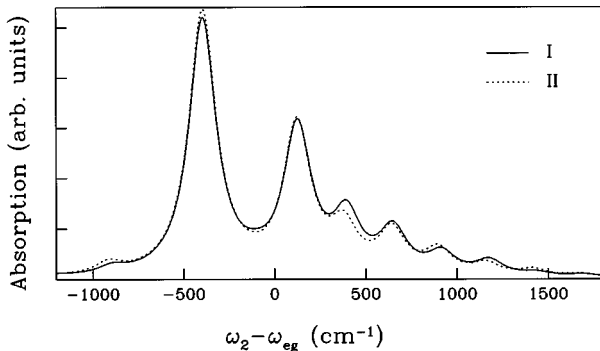


FIG. 7. Absorption spectra vs the detuning of the visible excitation for the parameters given in the entries labeled I and II of Table I.

the normal modes in the ground electronic state, their displacements in the excited state, their infrared absorption strengths, their frequencies in the excited state, and the mode mixing angle. When the model is being restricted to linear vibronic couplings only, the frequencies of the vibrational modes are identical in both electronic states and the Dushinsky rotation angle vanishes. This is the case for the last three entries to Table I which show the numerical results obtained from the least square fits. The spectra are drawn in Figs. 7–9, where the full lines are being used to show the result from the full quadratic model. The dotted lines correspond to the set of linear parameters listed in Table I with the labels indicated on the plots.

Let us first consider the visible absorption spectrum shown in Fig. 7. Of course, the fit with the linear model does not reproduce exactly the spectrum of our quadratic system, but the difference is rather small. From Table I, we see that this was achieved with normal mode frequencies closer to the excited state values than to the ground state values of the reference model, and by changing the displacements by up to 50%.

Next, we turn to the SFG spectra as a function of the infrared frequency depicted in Fig. 8. The upper half of the plot shows that the result of the fit with the linear model is extremely satisfactory and Table I tells us that the frequen-

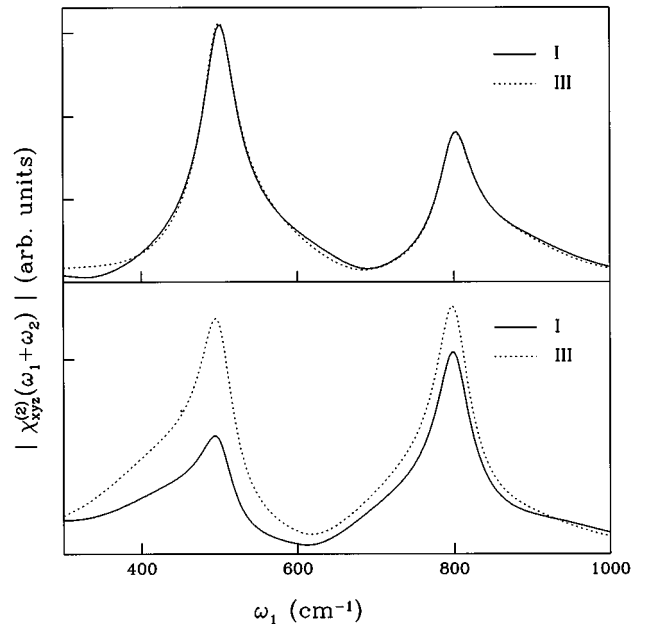


FIG. 8. SFG spectra vs the infrared frequency, for the parameters given in the entries labeled I and III of Table I. The upper and lower halves correspond, respectively, to a visible frequency of $20\,000\text{ cm}^{-1}$ and $20\,500\text{ cm}^{-1}$.

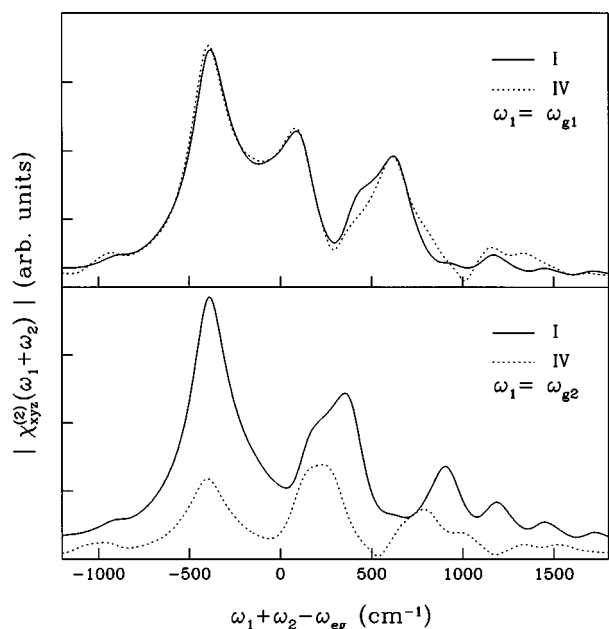


FIG. 9. SFG spectra vs the detuning of the visible frequency. The infrared excitation is resonant with $\omega_{g,1}=500\text{ cm}^{-1}$ transition in the upper half, and with the $\omega_{g,2}=800\text{ cm}^{-1}$ transition in the lower half. The other parameters are given in the caption and in the entries labeled I and IV of Table I.

cies of the modes and the intensities of both infrared transitions have been recovered very well. In fact, changing the value of the displacement of the first vibrational mode has been enough to make the two spectra agree. However, if we keep the parameters that have been determined in this way, and shift the frequency of the visible source by 500 cm^{-1} , then the linear and the quadratic models lead to completely different relative intensities of the peaks. This is what is being shown in the lower part of Fig. 8. Conversely, had we performed the fit in the second situation, we would have obtained parameters which would not suit the first experiment at all. Hence, in principle at least, it appears that it is possible to determine the need for a quadratic model provided that one performs several such spectra for different wavelengths of the visible excitation.

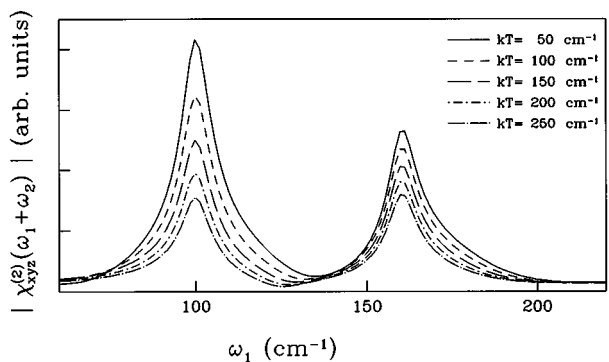


FIG. 10. SFG spectra vs the infrared frequency for various values of the thermal energy kT . The set of parameters used here are those of Fig. 3 divided by a factor 5, except the electronic transition frequency.

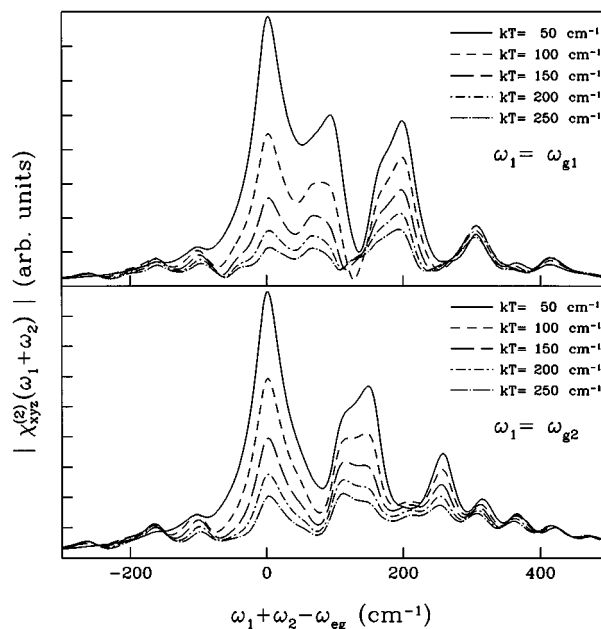


FIG. 11. SFG spectra vs the detuning of the visible frequency for different temperatures presented as in Fig. 10.

Finally, in Fig. 9, we represent DR IRVSFG spectra drawn vs a linear function of the frequency of the visible beam, the infrared source exciting resonantly one or the other vibrational mode. This type of spectroscopy leading to more resonance features, the fit shown in the upper half of the plot is somewhat more difficult to achieve but it succeeds to a good extent. However, Table I shows that the parameters found differ greatly from the first entry. The frequency of the second mode is off by a wide margin and the derivative of the permanent dipole moment with respect to the relevant normal coordinate has doubled in absolute value and even changed sign. In the lower part of Fig. 9 we show that the linear parameter set is inconsistent with the spectra recorded while resonantly exciting the second mode. We are thus led to the conclusion that while the second type of spectroscopy is more sensitive to changes in parameters, it still requires us to perform fits of several spectra to determine whether quadratic effects are present. More importantly, a single spectrum may accommodate the linear model sufficiently well, but lead to erroneous values for the parameters.

Let us mention here that we have also performed least square fits with the full set of both linear and quadratic parameters, typically using the values obtained from the previous fits as initial guesses, to verify that the program always converged back to the initially chosen quadratic model.

To close this section on numerical simulations, let us examine the behavior of DR IRVSFG spectra as a function of temperature. In order to work with a reasonable temperature scale, the frequencies of the vibrational modes have been divided by 5 in the following simulations. All the other parameters are as in entry I of Table I. The SFG spectrum vs the infrared frequency is depicted in Fig. 10 for five different temperatures as indicated on the plot. Notice that the electronic and vibrational dephasing constants introduced in the beginning of this section have also been divided by 5 and do not depend on temperature. Hence, the widths of the resonance features in the spectra do not change, and the effect of

the temperature as depicted here reflects only the changes in populations of the various vibrational levels of the molecule.

We observe an overall decrease in intensity of the signal with increasing temperature linked to the diminishing difference in population between a given vibronic state and the state with just one more quantum of vibration. We further notice that the peak corresponding to the 100 cm^{-1} mode is affected more than the resonance due to the 160 cm^{-1} mode, as expected. This observation helps to understand the SFG spectra vs the frequency of the visible excitation drawn in Fig. 11. Again, in addition to an overall decrease in intensity of the signal, we observe changes in the relative heights of the various peaks, the resonances corresponding to the higher frequency mode being less sensitive to an increase in temperature.

V. CONCLUSION

In the present work we have presented a general theoretical approach to evaluate doubly resonant infrared-visible sum-frequency generation from adsorbed species with general quadratic couplings. The model is valid at any temperature and may include as many vibrational modes as necessary. In the case of a model system restricted to two normal modes, we have shown that quadratic vibronic couplings may have an effect on the spectra that is comparable to that of linear parameters. We have considered both cases where either the infrared or the visible sources are tunable, and have shown that spectra plotted vs the frequency of the visible excitation are more sensitive to the coupling parameters mainly because of their richer features. However, it may be

expected that should there be many close lying active vibrational modes, it would be advantageous to consider the simpler infrared spectroscopy.

Concerning the problem of parameter recovery from experimental data, we can conclude that we have shown the ability of DR IRVVSF spectra to make it possible to discriminate between linear and quadratic vibronic coupling schemes, provided that one has access to a set of spectra corresponding to different wavelengths of the fixed frequency source. Indeed, we have demonstrated that a fit of one given spectrum with a linear model may very well appear to succeed while giving the wrong parameters. It follows that it is generally necessary to include the second-order terms of the vibrational Hamiltonian, namely the frequency shifts and the Duschinsky rotation. One can then hope to characterize the excited state potential surface of adsorbed species, provided that it remains harmonic. And should anharmonicity play a role, then one will need to show that the general quadratic Hamiltonian is inadequate to explain the results. This is an important step to take before using time resolved experiments to study the dynamics in the excited states of such systems.

ACKNOWLEDGMENTS

One of us (J.C.V.) wishes to thank Professor Bassani and Professor Tosi for their kind hospitality at the Scuola Normale Superiore in Pisa. This work was supported in part by the European Economic Community ‘Human Capital & Mobility’ Program, Contract No. ERBCHBGCT930355.

-
- [1] *Vibrational Spectroscopy of Molecules on Surfaces*, edited by J.T. Yates and T.E. Madey (Plenum Press, New York, 1987).
- [2] J.Y. Huang and Y.R. Shen, *Phys. Rev. A* **49**, 3973 (1994).
- [3] Soo-Y. Lee and E.J. Heller, *J. Chem. Phys.* **71**, 4777 (1979).
- [4] D.J. Tannor and E.J. Heller, *J. Chem. Phys.* **77**, 202 (1982).
- [5] Y.R. Shen, *Nature (London)* **337**, 519 (1989).
- [6] S. Mukamel and R.F. Loring, *J. Opt. Soc. Am. B* **3**, 595 (1986).
- [7] Z.F. Deng and S. Mukamel, *J. Chem. Phys.* **85**, 1738 (1986).
- [8] K.M. Chen and C.C. Pei, *Chem. Phys. Lett.* **165**, 523 (1990).
- [9] F. Duschinsky, *Acta Physicochim. URSS* **7**, 551 (1937).
- [10] A. Held, B.B. Champagne, and D.W. Pratt, *J. Chem. Phys.* **95**, 8732 (1991).
- [11] V. Hizhnyakov and I. Tehver, *Opt. Commun.* **32**, 419 (1980).
- [12] R. Kubo and Y. Toyozawa, *Prog. Theor. Phys.* **13**, 160 (1955).
- [13] J.B. Page and D.L. Tonks, *J. Chem. Phys.* **75**, 5694 (1981).
- [14] C.K. Chan and J.B. Page, *J. Chem. Phys.* **79**, 5234 (1983); *Chem. Phys. Lett.* **104**, 609 (1984).
- [15] C.K. Chan, J.B. Page, D.L. Tonks, O. Brafman, B. Khodadost, and C.T. Walker, *J. Chem. Phys.* **82**, 4813 (1985).
- [16] H.M. Lu and J.B. Page, *Chem. Phys. Lett.* **131**, 87 (1986); *J. Chem. Phys.* **88**, 3508 (1988).
- [17] D.L. Tonks and B.G. Dick, *Phys. Rev. B* **19**, 1136 (1979); **19**, 1149 (1979).
- [18] D.L. Tonks, *Phys. Rev. B* **22**, 6420 (1980).
- [19] D.L. Tonks and J.B. Page, *Chem. Phys. Lett.* **79**, 247 (1981).
- [20] J.C. Vallet, A.J. Boeglin, J.P. Lavoine, and A.A. Villaeys, *J. Chin. Chem. Soc.* **42**, 195 (1995).
- [21] J.C. Vallet, A.J. Boeglin, J.P. Lavoine, and A.A. Villaeys, *Chem. Phys. Lett.* **241**, 203 (1995).
- [22] Y. Fujimura and S.H. Lin, *J. Chem. Phys.* **71**, 3733 (1979).
- [23] S.H. Lin, R.G. Alden, R. Islampour, H. Ma, and A.A. Villaeys, *Density Matrix Methods and Femtosecond Processes* (World Scientific, Singapore 1991).
- [24] S.H. Lin, R.G. Alden, A.A. Villaeys, and V. Pflumio, *Phys. Rev. A* **48**, 3137 (1993).
- [25] A.A. Villaeys, V. Pflumio, and S.H. Lin, *Phys. Rev. A* **49**, 4996 (1994).
- [26] J.C. Vallet, A.A. Villaeys, J.P. Lavoine, and S.H. Lin, *Chem. Phys.* **189**, 657 (1994).
- [27] S.H. Lin and A.A. Villaeys, *Phys. Rev. A* **50**, 5134 (1994).
- [28] V. Pflumio, J.C. Vallet, A.J. Boeglin, A.A. Villaeys, and J.P. Lavoine, *Phys. Rev. A* **51**, 3174 (1995).
- [29] D.L. Tonks and J.B. Page, *J. Chem. Phys.* **88**, 738 (1988).
- [30] H.M. Lu and J.B. Page, *J. Chem. Phys.* **90**, 5315 (1989).
- [31] H.M. Lu and J.B. Page, *J. Chem. Phys.* **92**, 7038 (1990).
- [32] R. Islampour, M. Hayashi, and S.H. Lin, *Chem. Phys. Lett.* **234**, 7 (1995).
- [33] X.D. Zhu, Hajo Suhr, and Y.R. Shen, *Phys. Rev. B* **35**, 3047 (1986).
- [34] F. Venuti and G. Marconi, *J. Mol. Struct.* **266**, 235 (1992).